

---

# DISPERSION FORCES STABILISE ICE COATINGS AT CERTAIN GAS HYDRATE INTERFACES WHICH PREVENT WATER WETTING

---

A PREPRINT

**M. Boström\***

Department of Energy and Process Engineering  
Norwegian University of Science and Technology  
NO-7491 Trondheim, Norway  
mathias.a.bostrom@ntnu.no

**R. Corkery<sup>†</sup>**

Surface and Corrosion Science  
Department of Chemistry  
KTH Royal Institute of Technology  
SE 100 44 Stockholm, Sweden  
corkery@kth.se

**E. R. A. Lima**

Programa de Pós-graduação em Engenharia Química  
Universidade do Estado do Rio de Janeiro  
CEP 20550-013, Rio de Janeiro RJ, Brazil

**O. I. Malyi**

Centre for Materials Science and Nanotechnology  
Department of Physics  
University of Oslo  
P. O. Box 1048 Blindern  
NO-0316 Oslo, Norway

**S. Y. Buhmann<sup>‡</sup>**

Physikalisches Institut  
Albert-Ludwigs-Universität Freiburg  
Hermann-Herder-Str. 3  
79104 Freiburg, Germany

**C. Persson**

Centre for Materials Science and Nanotechnology  
Department of Physics  
University of Oslo  
P. O. Box 1048 Blindern  
NO-0316 Oslo, Norway

**I. Brevik**

Department of Energy and Process Engineering  
Norwegian University of Science and Technology  
NO-7491 Trondheim, Norway

**D. F. Parsons**

School of Engineering and IT  
Murdoch University  
90 South St  
Murdoch, WA 6150, Australia  
d.parsons@murdoch.edu.au

**J. Fiedler<sup>§</sup>**

Physikalisches Institut  
Albert-Ludwigs-Universität Freiburg  
Hermann-Herder-Str. 3  
79104 Freiburg, Germany  
johannes.fiedler@physik.uni-freiburg.de

March 1, 2022

---

\*Centre for Materials Science and Nanotechnology, Department of Physics, University of Oslo, P. O. Box 1048 Blindern, NO-0316 Oslo, Norway

<sup>†</sup>Applied Physical Chemistry, KTH Royal Institute of Technology, SE 100 44 Stockholm, Sweden

<sup>‡</sup>Freiburg Institute for Advanced Studies, Albert-Ludwigs-Universität Freiburg, Albertstr. 19, 79104 Freiburg, Germany

<sup>§</sup>Centre for Materials Science and Nanotechnology, Department of Physics, University of Oslo, P. O. Box 1048 Blindern, NO-0316 Oslo, Norway

## ABSTRACT

Gas hydrates formed in oceans and permafrost occur in vast quantities on Earth representing both a massive potential fuel source and a large threat in climate forecasts. They have been predicted to be important on other bodies in our solar systems such as Enceladus, a moon of Saturn.  $\text{CO}_2$ -hydrates likely drive the massive gas-rich water plumes seen and sampled by the spacecraft Cassini, and the source of these hydrates is thought to be due to buoyant gas hydrate particles. Dispersion forces cause gas hydrates to be coated in a 3-4 nm thick film of ice, or to contact water directly, depending on which gas they contain. These films are shown to significantly alter the properties of the gas hydrate clusters, for example, whether they float or sink. It is also expected to influence gas hydrate growth and gas leakage.

**Keywords** Gas hydrates · Interfacial ice formation · Buoyancy · Lifshitz interactions · Dispersion forces

## 1 Introduction

Gas hydrates are systems consisting of water and gas molecules forming a solid ice structure. Such systems can naturally be found in ice-cold water [1]; in particular, they can occur in permafrost [2], sediments [3], and below the oceans in the seabed [4]. For the latter, there are particularly interesting examples where gas hydrates are considered important in connection with planetary processes and the implications for life. The aqueous ocean-bearing moons Europa and Enceladus are perhaps the best examples in our solar system beyond Earth where gas hydrates are formed in salty oceans that are favourable for life [5]. On Mars, methane distribution is associated with subterranean water, implying the presence of methane hydrates [6]. On Enceladus giant plumes of erupted gases are observed and the composition directly measured to be water, salts and volatile gases including  $\text{CO}_2$ ,  $\text{CO}$ ,  $\text{N}_2$ ,  $\text{H}_2\text{S}$  and methane [7, 8]. Several hypotheses consider gas hydrates to be important for the creation of volatile enriched plumes and for the composition of ice layers beneath and/or entrained into, or sprayed onto the outer surface of Enceladus [9, 10, 11]. In particular, type II gas hydrates on Enceladus and Europa are calculated to be less dense than water and can float in their respective oceans. They are thereby available for incorporation into the overlying thick ice layer of each icy moon. Type I  $\text{CO}_2$  hydrates are at a density where their positive or negative buoyancy is uncertain [12, 13, 14, 15, 9]. However, if a layer of water ice forms on these gas hydrates in the presence of ice cold liquid water, then the growth of such hydrate crystals may be limited by the capping effect. This may have an impact on their buoyancy, and thus on the hypothesized composition of the ice layers in Enceladus and Europa, with obvious implications for the composition of their plumes and their potential to sample the underlying oceans and any harboured life.

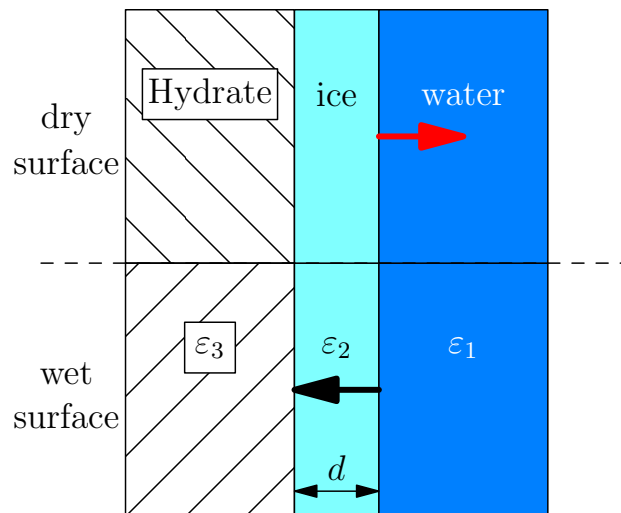


Figure 1: (Color online). Schematic figure of the considered arrangement. A gas hydrate surface ( $\epsilon_3$ ) on the left, separated by an ice layer ( $\epsilon_2$ ) of thickness  $d$  from a water layer ( $\epsilon_1$ ). A dry surface feels a repulsive Casimir force at the ice-water interface which yields a stable ice interface. In contrast, an attractive force results in a wet surface due to the vanishing of the ice interface.

On Earth, methane hydrates occur naturally and in engineered situations. Large reservoirs of methane hydrates occur in sediments of deep oceans basins, at shallower depths in the sediments of arctic sea shelves, and in deep permafrost regions. In all these cases, the understanding of whether a layer of ice forms on the hydrate has implications for exploration and production of fossil fuels, and also for understanding the potential for methane contribution to greenhouse gases as the planet becomes warmer.

In all of the contexts above, hydrates are usually surrounded by ice cold water. Depending on the gas hydrate structure with respect to contributions and volume fractions, it turns out that some hydrates form an ice interface to water, whereas others do not. The latter have a wet surface. The ones with a gas hydrate-ice interface may be considered to have a dry surface. The prediction of the wet or dry surface cannot be made easily. In the present paper we address this issue by considering a planar three-layer system, as depicted in Fig. 1, namely a gas hydrate layer, an ice sheet, and a water layer. Thus, we assume that initially all hydrates are covered by an ice interface. We estimate the Casimir force acting on the outside at the ice-water interface, i.e., the pressure acting on the system. Depending on the sign of the Casimir force, it will work towards growth or melting of the thin ice sheet. We assume that the temperature is at the triple point of water. An attractive pressure acting on the ice layer thus results in a melting of the ice sheet [16, 17, 18]. It will simply vanish. This kind of consideration is not new. In the past, ice melting at the triple point with a nano-sized film of water was discussed [19]. It was found that a thin water film is energetically favourable up to a certain thickness where it has an energy minimum [19, 20, 21, 22, 23]. The inclusion of retardation resulted in incomplete melting while a non-retarded approximation predicted complete melting for an ice surface at the triple point of water [19].

Here we apply Lifshitz theory to estimate the energy of the hydrate-ice-system as a function of ice thickness, and show that for some gas hydrates the ice film is stabilised at a thickness of 3-4 nm, while for other gas hydrates the ice film is unstable, resulting in direct wetting.

## 2 Materials and Methods

### 2.1 Dispersion forces between solid bodies

The Casimir interaction energy  $F(d)$  (also known as Lifshitz free energy) per unit area between material 1 (water) with dielectric function  $\varepsilon_1$  and material 3 (gas hydrate),  $\varepsilon_3$ , separated by the distance  $d$  across medium 2 (ice),  $\varepsilon_2$  as depicted in Fig. 1 can be written at temperature  $T$  as [24, 25, 26, 27]

$$F(d) = \sum_{n=0}^{\infty} ' [g^{\text{TM}}(\xi_n) + g^{\text{TE}}(\xi_n)] , \quad (1)$$

where  $g^{\text{TX}}(\xi)$  (TX=TM, TE) denotes the trace over the scattering for transverse magnetic (TM) and transverse electric (TE) Green's function. This fundamental solution comes from the vector Helmholtz equation for the electric field. The primed sum denotes that the  $n = 0$  term is weighted by a factor one half. At finite temperature these functions are evaluated at the discrete Matsubara frequencies  $\xi_n = 2\pi n k_B T / \hbar$  [28]. The systems in this study, as mentioned, are all studied at the triple point of water. For the considered three layer system, the traces over the scattering Green's functions, including multiple reflection in the center layer, can be written (in cgs units) as

$$g^{\text{TX}}(\xi_n) = \frac{1}{\beta} \int \frac{d^2 q}{(2\pi)^2} \ln \{ 1 - e^{-2\gamma_2 d} r_{12}^{\text{TX}} r_{32}^{\text{TX}} \} , \quad (2)$$

with  $\beta = 1/(k_B T)$ , and the Fresnel reflection coefficients are

$$r_{i2}^{\text{TM}} = \frac{\varepsilon_i \gamma_2 - \varepsilon_2 \gamma_i}{\varepsilon_i \gamma_2 + \varepsilon_2 \gamma_i} , \quad (3)$$

for TM waves and

$$r_{i2}^{\text{TE}} = \frac{\gamma_2 - \gamma_i}{\gamma_2 + \gamma_i} , \quad (4)$$

for TE waves. We have introduced the imaginary part of the transverse wave vector  $\gamma_i^2 = q^2 + \xi^2 \varepsilon_i / c^2$ . We assume nonmagnetic media.

### 2.2 Material Modelling

Dielectric functions (at imaginary frequencies) were taken from Elbaum and Schick [19] using the data from Daniels [29] and labeled by ice<sub>JD</sub> and from Seki et al.[30] (ice<sub>SM</sub>) for ice ( $\varepsilon_2$ ) and from Elbaum and Schick[19] for water ( $\varepsilon_1$ ). These dielectric functions are for a system at the triple point of water, close to zero degrees Celsius at low pressure.

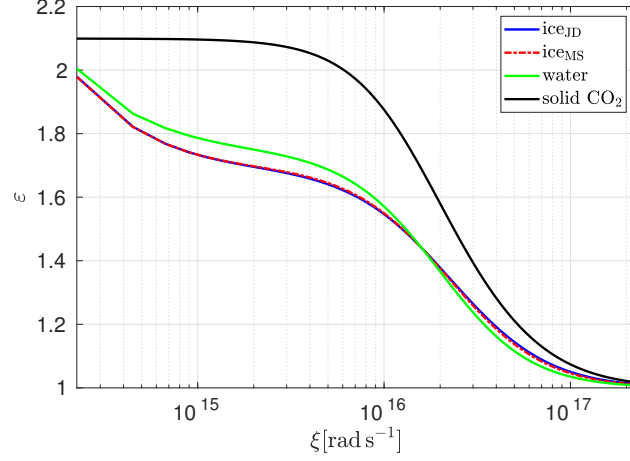


Figure 2: (Color online) The dielectric functions of crystalline CO<sub>2</sub>[31], both ice models and water [19] at 273.16 K.

The final results for ice melting [19, 20, 21, 22, 23, 31, 32] and water freezing [33, 34] are sensitive to the dielectric functions of ice and water since these are extremely similar when the water is in equilibrium with the ice. We show in Fig. 2 the dielectric functions for crystalline CO<sub>2</sub>, water and ice.

A model for the dielectric function of a gas hydrate ( $\epsilon_3$ ) is derived using the Lorentz-Lorenz model [35] with the mixing scheme specifically for gas hydrates taken from Bonnefoy et al.[36, 37]

$$\epsilon_3 = \frac{1 + 2\Gamma}{1 - \Gamma}, \quad (5)$$

with

$$\Gamma = \frac{\epsilon_2 - 1}{\epsilon_2 + 2} \left( \frac{n_{\text{wh}}}{n_i} \right) + \frac{4\pi\alpha_M n_M}{3}, \quad (6)$$

which means that the dominating factors for the dielectric function of gas hydrates are the ice polarisability weighted by density of water in the hydrate relative to pure ice, and the polarisabilities of different gas molecules weighted by their corresponding densities. The mass density of water in pure ice is 0.9167 g/cm<sup>3</sup> [38], giving the number density of water molecules in pure ice as  $n_i = 3.06 \times 10^{-2} \text{ \AA}^{-3}$ . The number densities of gas molecules ( $n_M$ ) and water molecules ( $n_{\text{wh}}$ ) in different gas hydrate structures are tabled in Tab. 1 with the water/gas number density ratio

$$p = \frac{n_{\text{wh}}}{n_M}. \quad (7)$$

Quantum chemical calculations of dynamic polarisabilities at discrete frequencies were represented at arbitrary imaginary frequencies  $i\xi$  by fitting to the oscillator model,

$$\alpha_M(i\xi) = \sum_j \frac{\alpha_j}{1 + (\xi/\omega_j)^2} \quad (8)$$

A 5-mode fit has previously been found to describe the dynamic polarisability accurately to a 0.02% relative error [41]. The adjusted parameters for a 5-mode model for CO<sub>2</sub>, CH<sub>4</sub>, N<sub>2</sub>, and H<sub>2</sub>S are given in our recent work [42]. Quantum

Table 1: Hydrate mass densities ( $\rho_h$ ) and number densities of water ( $n_{\text{wh}}$ ) and gas molecules ( $n_M$ ) in different gas hydrates. The water/gas number density ratio is denoted  $p$ .

Gas molecule	$p$	$\rho_h$ (g/cm <sup>3</sup> )	$n_M$ (Å <sup>-3</sup> )	$n_{\text{wh}}$ (Å <sup>-3</sup> )
CO <sub>2</sub> , [39]	5.75	1.13	$4.61 \times 10^{-3}$	$2.65 \times 10^{-2}$
CO <sub>2</sub> , [39]	7.67	1.05	$3.47 \times 10^{-3}$	$2.66 \times 10^{-2}$
CO <sub>2</sub> , [40]	6.0	1.117	$4.42 \times 10^{-3}$	$2.65 \times 10^{-2}$
CH <sub>4</sub> , [2]	5.75	0.90	$4.53 \times 10^{-3}$	$2.60 \times 10^{-2}$
CH <sub>4</sub> , [40]	6.0	0.91	$4.41 \times 10^{-3}$	$2.65 \times 10^{-2}$
H <sub>2</sub> S, [40]	7.0	1.044	$3.92 \times 10^{-3}$	$2.75 \times 10^{-2}$
N <sub>2</sub> , [40]	6.0	0.995	$4.4 \times 10^{-3}$	$2.64 \times 10^{-2}$

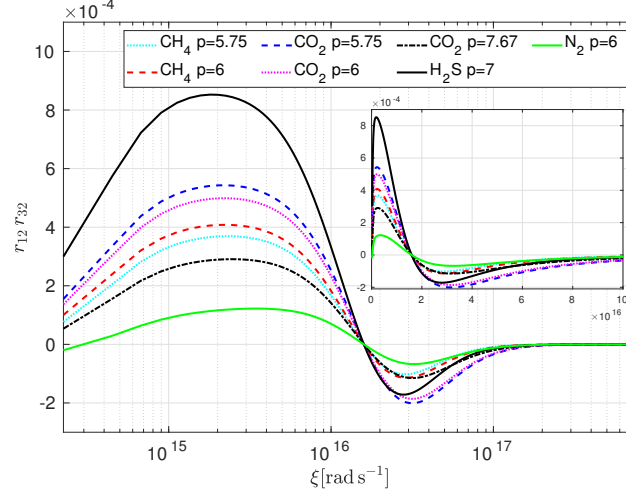


Figure 3: (Color online) Product of the non-retarded reflection coefficients for the two interfaces. Here we show these for the three  $\text{CO}_2$  gas hydrates and the two  $\text{CH}_4$  gas hydrates that we consider (the inset shows the same on a linear scale).

calculations on which the fits were based were taken at a coupled-cluster singles and doubles (CCSD) level of theory [43] using aug-cc-pVQZ basis sets [44].

### 2.3 Product of Reflection Coefficients

As can be observed in Eq. (2), the Casimir force is determined by the product of reflection coefficients at both interfaces, summed over all frequencies. Thus, the magnitude and sign is given by the balance of areas enclosed by these curves above and below the frequency axis. This behaviour is illustrated in Fig. 3, where the products of the non-retarded Fresnel coefficients (TM mode) are shown each given by

$$r_{i2} = \frac{\varepsilon_i - \varepsilon_2}{\varepsilon_i + \varepsilon_2}. \quad (9)$$

One can get insights from this quantity also in cases where retardation matter. Negative values for the product shown in Fig. 3 (larger in magnitude for  $\text{CO}_2$  hydrates than for  $\text{CH}_4$  hydrates) for high frequencies contribute to repulsion. The crossing point at  $1.6 \times 10^{16} \text{ rad s}^{-1}$  where  $r_{12}r_{32} = 0$  corresponds to the frequency where the dielectric function of ice crosses that of pure water, seen in Figure 2. For nonretarded, small film thicknesses, the respective sum over all frequencies (with many more terms for high frequencies than for low frequencies) gives the net sign for the free energy of very thin ice films. Retardation favours the small-frequency contributions and hence screens out high frequency (repulsive) contributions for thicker ice films. It turns out that already for film thicknesses as thin as a few nanometers retardation is important for ice-water related systems [19]. The net sign in our case is not trivial, and we will demonstrate later that  $\text{CO}_2$  and  $\text{N}_2$  hydrates in water behave differently from  $\text{CH}_4$  and  $\text{H}_2\text{S}$  hydrates in water.

## 3 Results

### 3.1 Gas hydrate specific ice formation

While it is well known that water can start to freeze from its surface when the temperature goes to zero degrees Celsius, Elbaum and Schick [33] predicted that dispersion forces do not play a role in this mechanism. In fact, they found that a thin ice film on the surface would have its energy minimum for zero ice film thickness which would not result in surface freezing on open water surfaces. The underlying mechanism for why ice growth actually occurs at the surface is that large ice structures float with a certain fraction above a water surface due to the lower density of ice. In contrast to their results, we have found that buoyancy combined with dispersion and double layer forces establish an equilibrium where large ice particles float on the surface while small (micron-sized) ice particles are trapped at a distance below a water surface [45]. Further, it was shown that ice formation can be induced by dispersion forces near silica-water interfaces (where silica can be used as a model for rock material) [34].

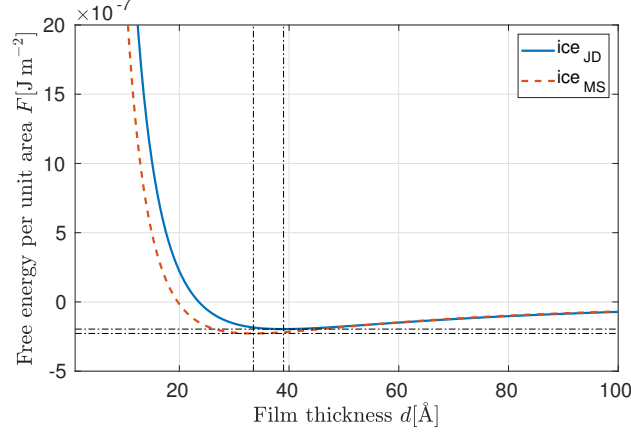


Figure 4: (Color online) The free energy per unit area (at 273.16 K) as a function of ice film thickness on the boundary between the surface of a crystalline  $\text{CO}_2$  structure and liquid water. It is predicted that at equilibrium an ice film around  $d = 33 \text{ \AA}$  for the ice model from M. Seki *et al.* and  $d = 39 \text{ \AA}$  for J. Daniels' model.

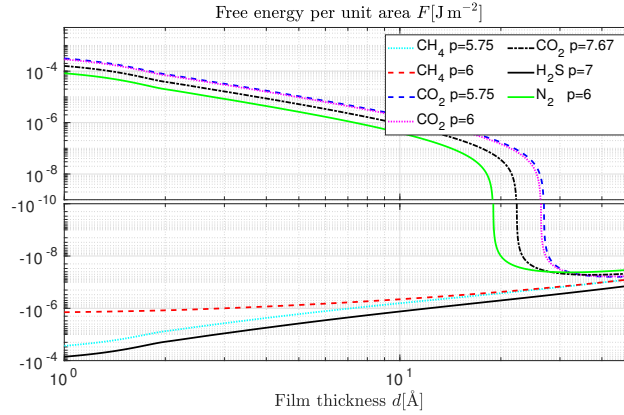


Figure 5: (Color online) The Lifshitz free energy per unit area (at 273.16 K) for a flat three-layer system (water-ice-gas hydrate) as a function of the ice film thickness  $d$ . For  $\text{CO}_2$  gas hydrates and the  $\text{N}_2$  gas hydrate, energy minimum exist corresponding in each case to an equilibrium ice film thickness:  $d_{\text{CO}_2} = 44, 43$  and  $37 \text{ \AA}$  for  $\text{CO}_2$  volume fractions  $p = 5.75, 6$  and  $7.67$ , respectively, and  $d_{\text{N}_2} = 32 \text{ \AA}$ .

Before presenting the gas hydrates, we first use the dielectric functions shown in Fig. 2 to perform calculations for the free energy for an ice film growing on an interface between crystalline  $\text{CO}_2$  and ice cold water. We see in Fig. 4 that this three layer system has an energy minimum corresponding to an equilibrium ice film with thickness ( $d$ ) between 3.3 nm and 3.9 nm, depending on the model for the dielectric function of ice. In the remainder of this letter, we use  $\text{ice}_{\text{JD}}$ , the Daniels [29] model for ice, since both models give very similar results. The thicknesses correlate with the frequency where the dielectric functions of ice and water have a crossing [34].

Figure 5 shows the free energy as a function of ice film thickness for different gas hydrates in ice cold water. Ice films are predicted for  $\text{CO}_2$  hydrates ( $d = 44, 43$  and  $37 \text{ \AA}$  for volume fractions  $p = 5.75, 6$  and  $7.67$ , respectively) and for the  $\text{N}_2$  hydrate ( $d = 32 \text{ \AA}$ ) but not for any of the  $\text{CH}_4$  or  $\text{H}_2\text{S}$  hydrates. In the former cases, retardation plays a role at the nanometer scale as it is the reason for the change in the sign of the Lifshitz energy. This model is sensitive to the various dielectric functions which are involved in the system [46]. While the results are model dependent for the specific combination of materials used, the clear trend is that interfacial ice caps can exist at some gas hydrates in ice cold water, but not for others.

The stark difference in behaviour between  $\text{CO}_2$  or  $\text{N}_2$  hydrates and  $\text{CH}_4$  or  $\text{H}_2\text{S}$  hydrates can be understood from differences in gas polarisability in the optical/UV spectrum, combined with the difference in the dielectric spectra of water and ice. These are expressed in the maximum and minimum seen in the product of reflection coefficients in Figure 3. The positive value of the product  $r_{12}r_{32}$  at low frequencies contributes to stabilisation of the water interface

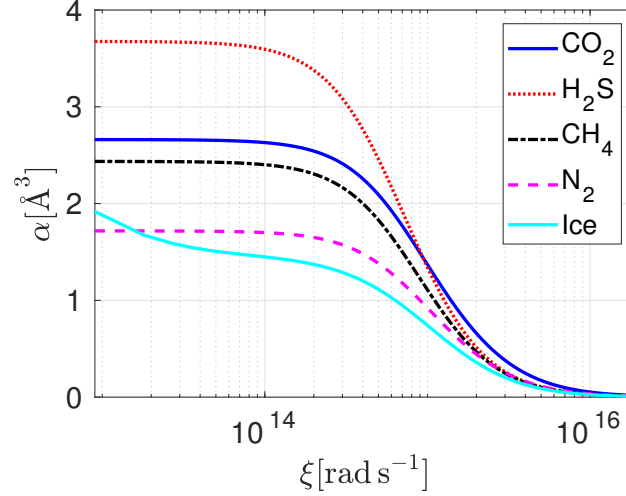


Figure 6: (Color online) Polarisabilities of gas molecules at imaginary frequencies. The polarisability of a water molecule in ice is also shown for comparison.

towards the hydrate interface, i.e., wetting, with removal of the ice layer. Negative values at high frequencies destabilise the water interface, i.e., stabilise the ice layer. The overall behaviour is a balance between these two regimes. As discussed above, the positive and negative regimes ultimately derive from the reflection coefficient  $r_{12}$  between liquid water and ice, that is from the crossing in the dielectric functions of ice and cold water at  $1.6 \times 10^{16} \text{ rad s}^{-1}$  seen in Figure 2. The effect of the hydrate (via reflection coefficient  $r_{32}$ ) is to strengthen or attenuate  $r_{12}$ . Figure 3 shows that the high frequency stabilisation of the ice layer is weaker for  $\text{CH}_4$  and  $\text{N}_2$  than for  $\text{CO}_2$  at all hydrate ratios, while  $\text{H}_2\text{S}$  is only weaker than  $\text{CO}_2$  at higher water/gas ratios. At low frequencies, destabilisation of the ice layer is much stronger for  $\text{H}_2\text{S}$  than  $\text{CO}_2$ , while weaker for  $\text{N}_2$ . In the balance between low frequency destabilisation and high frequency stabilisation of the ice layer, high frequencies dominate for  $\text{CO}_2$ , but are insufficiently weak for  $\text{CH}_4$ . In the case of  $\text{N}_2$ , low frequency behaviour is weaker than for other gases, so again high frequency stabilisation of ice dominates. In the case of  $\text{H}_2\text{S}$ , low frequency destabilisation of the ice layer is stronger than for  $\text{CO}_2$  and dominates over high frequency stabilisation. These patterns follow the underlying polarisabilities of the gas molecules, see Figure 6: the polarisability of  $\text{CH}_4$  is weaker than  $\text{CO}_2$  at all frequencies. The polarisability of  $\text{H}_2\text{S}$  is significantly stronger than  $\text{CO}_2$  at low frequencies, but drops rapidly at high frequencies, crossing  $\text{CO}_2$  to respond similarly to  $\text{CH}_4$  in the UV spectrum. The polarisability of  $\text{N}_2$  is much weaker than other gas molecules, in particular, is much closer to the polarisability of a water molecule. The polarisability per ice molecule is shown in Figure 6 for comparison. This results in an  $\text{N}_2$  gas hydrate dielectric function closer to that of ice, leading to a smaller reflection coefficient. Stabilisation of the ice layer at a hydrate surface is determined predominantly from the polarisability of the gas molecule relative to a water molecule in the optical spectrum around  $3 \times 10^{15} \text{ rad s}^{-1}$  (stabilising water wetting) and in the UV spectrum around  $3 \times 10^{16} \text{ rad s}^{-1}$  (stabilising the ice layer).

### 3.2 Size dependence for floating of gas hydrate clusters

Buoyancy of gas hydrate particles is of considerable importance for understanding the distribution and composition of ices, water and gases in subglacial water bodies in Antarctica and on ocean bearing moons of our solar systems and extra solar planets. Buoyancy of gas hydrates on these water bodies depends on hydrate density and assumed ocean densities.

Lake Vostok, located 4 km below the Antarctic surface, is an analogue of deeper subglacial oceans the Jovian and Saturnian moons and is a notable target for astrobiological studies. McKay et al. [12] suggest the observed lack of gas hydrates accreted at the top of Lake Vostok in Antarctica (density  $1.016 \text{ g cm}^{-3}$ ) is consistent with formation of relatively dense  $\text{CO}_2$  clathrate hydrates that sink to the lake floor. Mousis et al. (2013) later estimated the densities of type I and II clathrate  $\text{CO}_2$  hydrates in Lake Vostok, concluding that  $\text{CO}_2$ -containing type I clathrates sink above a critical  $\text{CO}_2$  composition in the lake.

Prieto-Ballesteros et al. [13] considered buoyancy of type I  $\text{CO}_2$ ,  $\text{SO}_2$ ,  $\text{CH}_4$  and  $\text{H}_2\text{S}$  gas hydrates (space group 223) on Europa, where two extreme models for the density of the ocean water were considered, namely a eutectic brine of composition  $\text{MgSO}_4\text{-H}_2\text{O}$  system with density  $1.19 \text{ g cm}^{-3}$  and a low salinity water ocean of density  $1.0 \text{ g cm}^{-3}$ . Safi

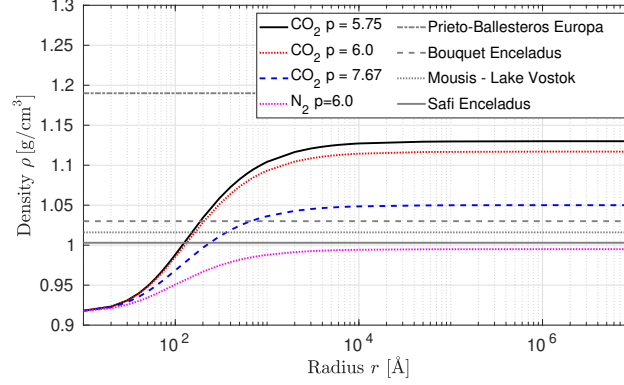


Figure 7: (Color online) The average densities of gas hydrate particles of varying radius for CO<sub>2</sub> hydrates with density fraction  $p = 5.75$  (solid black line),  $p = 6.0$  (dotted red line) and  $p = 7.67$  (dashed blue line) and N<sub>2</sub> with  $p = 6.0$  (dotted magenta line), each compositional variant coated in a layer of ice of thickness determined by the polarizability and amount of the entrapped gas species as specified above. As comparison we show the water densities in different systems. References for the water/gas number density ratios  $p$  are given in Tab. 1.

et al. [15] discuss the buoyancy of CO<sub>2</sub> hydrates using two further density estimates of the oceans of Europa (density 1.016 g cm<sup>-3</sup>) and Enceladus (1.003 g cm<sup>-3</sup>) and used measured gas hydrate densities. Bouquet et al. [9] consider the buoyancy of multiple guest clathrates on Enceladus using a calculated high pressure sea water density of 1.030 g cm<sup>-3</sup>, concluding the type I clathrates are marginally denser (1.040 g cm<sup>-3</sup>) than the sea water and type II significantly lighter (0.970 g cm<sup>-3</sup>).

Figure 7 shows the average densities of gas hydrate particles of varying radius, each compositional variant coated in a layer of ice of thickness determined by the polarizability and amount of the entrapped gas species. These were calculated using equation 10 below. The equilibrium ice film thicknesses and densities are given in the text immediately below Figure 5. The value used for the density of pure ice was 0.9167 g cm<sup>-3</sup>. Horizontal lines represent the estimated or measured density of the ocean/sea water on the various bodies.

It is quite apparent that for CO<sub>2</sub> gas hydrate particles, which are otherwise denser than most models for the water on Enceladus or in Lake Vostok, an equilibrium ice layer of the order of several nm has a significant impact on the buoyancy of the particles. When the radii of these is below approximately 20-100 nm, the average density drops below values estimated for the ocean water density on Enceladus and consequently will float. We use the following simple expression for the average density of a ice coated gas hydrate cluster (approximated as a sphere),

$$\rho_{av} = \frac{\rho_h r_h^3 + \rho_i [(r_h + d)^3 - r_h^3]}{(r_h + d)^3}. \quad (10)$$

Here  $\rho_{av}$  is the average density of mixed particle comprising a clathrate hydrate core and a shell of water ice,  $\rho_h$  densities are given in Tab. 1 for different gas hydrates,  $\rho_i$  is given for ice above, and  $r_h$  the radius of a gas hydrate cluster. Finally,  $d$  is the approximate thickness of each ice film at planar water-CO<sub>2</sub> gas hydrate and water-N<sub>2</sub> gas hydrate interfaces given above.

## 4 Conclusions

In analogy to the premelting layers of ice [19, 23, 22], we found that freezing of gas hydrates in ice cold water is caused by an energy minimum in dispersion energies. This is not expected at water surfaces [33] but predicted to occur at some water-solid interfaces [34]. We find that a significant difference between different gas hydrate surfaces in water lies in whether they are coated with a nano-sized interfacial ice cap or not. The result is sensitive to the details in the dielectric functions of the materials involved. However, our results indicate that some hydrates are more likely to have interfaces that are kept dry by an interfacial ice cap. We have seen this trend for three different volume fractions of CO<sub>2</sub> hydrates in water as well as for N<sub>2</sub> hydrate and crystalline CO<sub>2</sub> in water. Other hydrates, CH<sub>4</sub> hydrate in water, are more likely to stay wet and have no interfacial ice cap.

A review [47] a few years ago asked the question if gas hydrate surfaces in air are dry or wet. Our results are consistent with gas hydrate surfaces that are in equilibrium with water molecules in vapor phase. If a film of water is adsorbed on a gas hydrate surface, much thicker than say 10 nm, then our calculations can be extended to predict that a fraction of



that water will form an interfacial ice layer between the water film and the surface of the CO<sub>2</sub> (or N<sub>2</sub>) hydrates but not so for CH<sub>4</sub> (or H<sub>2</sub>S) hydrates. These differences for materials, whether their interfaces stay dry or wet, are expected to influence the fluxes of gas molecules into the liquid water and then further towards the surrounding atmosphere. Further, as we discussed above a dry surface may affect the growth and overall density of gas hydrate crystals. The density of type I CO<sub>2</sub> hydrate crystal densities are similar to that predicted for different ice coated ocean waters on Earth, Enceladus and Europa [12, 13, 14, 15, 9]. The density values in Tab. 1 for CO<sub>2</sub> hydrate suggest a water ice cap layer could make a significant difference in buoyancy when hydrate crystals have diameters in the range of approximately 20-100 nm, based on the 3-4 nm ice films we predict. Indeed if a layer of interfacial ice cap grows on a hydrate crystal early after nucleation, its growth may be restricted to such small sizes, leading to the formation of nanoscale, ice-capped CO<sub>2</sub> hydrate crystals with positive buoyancy.

Besides the requirement of accurate dielectric functions for quantitative predictions of such ice layer thicknesses, the restriction to interactions caused by dispersion forces yields a source of uncertainties. For non-polar systems, it would be sufficient to neglect electrostatic effects. However, water is a polar medium, thus interactions caused by permanent dipole moments will also play a role and will shift this theory to a more precise one. The extension of the theory of dispersion forces to include permanent dipole moments is of current interest for several groups and will also be part of further investigations. However, a simple estimation of such effects shows a small contribution to the dispersion forces which is smaller than in the vacuum case due to the shielding effect of the environmental medium.

We have notably shown that the above-mentioned density dependence of the gas hydrates induce a sinking or floating of the particles which is important for carbon capture and storage via gas hydrates [48]. The creation of an interfacial ice layer modify the average density of the particle, thus the buoyancy that determines the floating or sinking of the particle. When studying very small gas hydrates, the particle's curvature may be expected to play a role. It can easily be incorporated into theory by changing the geometry from a planar to a spherically layered system. However, since the size of the gas hydrate clusters are much larger than the predicted ice film layer a planar approximation is expected to give useful estimates. Such investigations will also effect the description of crystallization processes in particular for cloud creation [49] by treating the gas hydrate as cloud condensation nuclei.

## Acknowledgement

We gratefully acknowledge support from the Research Council of Norway (Project 250346), the German Research Council (grant BU 1803/6-1, S.Y.B. and J.F., BU 1803/3-1, S.Y.B.), the Research Innovation Fund by the University of Freiburg (S.Y.B., J.F.), the Freiburg Institute for Advanced Studies (S.Y.B.), and FAPERJ (JCNE E-26/203.223/2016). DFP acknowledges the grant of resources from the National Computational Infrastructure (NCI), which is supported by the Australian Government. Data available from authors.

## Disclaimer

This document is the unedited Author's version of a Submitted Work that was subsequently accepted for publication in ACS Earth and Space Chemistry, copyright © American Chemical Society after peer review. To access the final edited and published work see:

<https://doi.org/10.1021/acsearthspacechem.9b00019>

## References

- [1] Gerald R. Dickens and Mary S. Quinby-Hunt. Methane hydrate stability in seawater. *Geophysical Research Letters*, 21(19):2115–2118, 1994.
- [2] M. D. Max, editor. *Natural Gas Hydrate in Oceanic and Permafrost Environments*. Kluwer Academic Publishers, Washington DC, USA, 2003.
- [3] Tae-Hyuk Kwon, Gye-Chun Cho, and J. Carlos Santamarina. Gas hydrate dissociation in sediments: Pressure-temperature evolution. *Geochemistry, Geophysics, Geosystems*, 9(3), 2008.
- [4] Nariman Mahabadi, Xianglei Zheng, and Jaewon Jang. The effect of hydrate saturation on water retention curves in hydrate-bearing sediments. *Geophysical Research Letters*, 43(9):4279–4287, 2016.
- [5] F. Nimmo and R. T. Pappalardo. Ocean worlds in the outer solar system. *Journal of Geophysical Research: Planets*, 121:1378–1399, 2016.
- [6] S. Fonti and G. A. Marzo. Mapping the methane on Mars. *Astronomy and Astrophysics*, 512(A51):1–6, 2010.

- [7] J. H. Jr. Waite, M. R. Combi, W. H. Ip, T. E. Cravens, R. L. Jr. McNutt, W. Kasprzak, R. Yelle, Luhmann J., Niemann H., D. Gell, B. Magee, G. Fletcher, Lunine G., and W. L Tseng. Cassini ion and neutral mass spectrometer: Enceladus plume composition and structure. *Science*, 311(5766):1419–1422, 2006.
- [8] F. Postberg, J. Schmidt, Hillier J., S. Kempf, and R. Srama. A salt-water reservoir as the source of a compositionally stratified plume on Enceladus. *Nature*, 474(7353):620–622, 2011.
- [9] Alexis Bouquet, Olivier Mouis, J. Hunter Waite, and Sylvain Picaud. Possible evidence for a methane source in Enceladus’ ocean. *Geophysical Research Letters*, 42:1334–1339, 2015.
- [10] D. L. Matson, J. C. Castillo-Rogez, A. G. Davies, and T. V. Johnson. Enceladus: A hypothesis for bringing both heat and chemicals to the surface. *Icarus*, 221(1):53–62, 2012.
- [11] D. L. Matson, A. G. Davies, T. V. Johnson, T. B. Coimbe, J-P. and McCord, J. Radebaugh, and S. Singh. Enceladus’ near-surface CO<sub>2</sub> gas pockets and surface frost deposits. *Icarus*, 302:18–26, 2018.
- [12] C. P. McKay, K. P. Hand, P. T. Doran, D. T. Andersen, and J. C. Priscu. Clathrate formation and the fate of noble and biologically useful gases in lake vostok, antarctica. *Geophysical Research Letters*, 30(13), 2003.
- [13] O. Prieto-Ballesteros, J. S. Kargel, M. Fernandez-Sampedro, F. Selsis, E. S. Martinez, and D. L. Hogenboom. Evaluation of the possible presence of clathrate hydrates in europas icy shell or seafloor. *Icarus*, 177:491–505, 2005.
- [14] Olivier Mouis, Azzedine Lakhlifi, Sylvain Picaud, Matthew Pasek, and Eric Chassefiere. On the abundances of noble and biologically relevant gases in lake vostok, antarctica. *Astrobiology*, 13(4):380–390, 2013.
- [15] E. Safi, S. P. Thompson, A. Evans, S. J. Day, C. A. Murray, J. E. Parker, A. R. Baker, Oliveira J. M., and J. Th. van Loon. Properties of CO<sub>2</sub> clathrate hydrates formed in the presence of MgSO<sub>4</sub> solutions with implications for icy moons. *Astronomy and Astrophysics*, 600(A88):1–9, 2017.
- [16] L. D. Landau and E. M. Lifshitz. *Statistical Physics*. Butterworth-Heinemann, 1980.
- [17] Anders Nilsson and Lars G M Pettersson. The structural origin of anomalous properties of liquid water. *Nature Communications*, 6:8998, dec 2015.
- [18] J. E. Bertie, L. D. Calvert, and E. Whalley. Transformations of Ice II, Ice III, and Ice V at Atmospheric Pressure. *The Journal of Chemical Physics*, 38(4):840–846, 1963.
- [19] Michael Elbaum and M. Schick. Application of the theory of dispersion forces to the surface melting of ice. *Phys. Rev. Lett.*, 66:1713–1716, Apr 1991.
- [20] M. Elbaum, S.G. Lipson, and J.G. Dash. Optical study of surface melting on ice. *Journal of Crystal Growth*, 129(3):491 – 505, 1993.
- [21] L. A. Wilen, J. S. Wettlaufer, M. Elbaum, and M. Schick. Dispersion-force effects in interfacial premelting of ice. *Phys. Rev. B*, 52:12426–12433, Oct 1995.
- [22] J. G. Dash, H. Fu, and J. S. Wettlaufer. The premelting of ice and its environmental consequences. *Reports on Progress in Physics*, 58(1):115, 1995.
- [23] J. S. Wettlaufer. Impurity Effects in the Premelting of Ice. *Phys. Rev. Lett.*, 82:2516–2519, Mar 1999.
- [24] I.E. Dzyaloshinskii, E.M. Lifshitz, and L.P. Pitaevskii. The general theory of van der Waals forces. *Advances in Physics*, 10(38):165–209, 1961.
- [25] V. A. Parsegian. *Van der Waals forces: A handbook for biologists, chemists, engineers, and physicists*. Cambridge University Press, New York, 2006.
- [26] B. W. Ninham and P. Lo Nostro. *Molecular Forces and Self Assembly in Colloid, Nano Sciences and Biology*. Cambridge University Press, Cambridge, 2010.
- [27] S. Y. Buhmann. *Dispersion Forces I: Macroscopic quantum electrodynamics and ground-state Casimir, Casimir-Polder and van der Waals forces*. Springer, Heidelberg, 2012.
- [28] S Y Buhmann. *Dispersion Forces II: Many-Body Effects, Excited Atoms, Finite Temperature and Quantum Friction*. Springer Tracts in Modern Physics. Springer, Heidelberg, 2012.
- [29] J. Daniels. Bestimmung der optischen Konstanten von Eis aus Energie - Verlustmessungen von schnellen Elektronen. *Optics Communications*, 3(4):240 – 243, 1971.
- [30] Masami Seki, Koichi Kobayashi, and Jun’ichirō Nakahara. Optical Spectra of Hexagonal Ice. *Journal of the Physical Society of Japan*, 50(8):2643–2648, 1981.

- [31] P. Thiyam, E. R. A. Lima, O. I. Malyi, D. F. Parsons, S. Y. Buhmann, C. Persson, and M. Boström. Effects of van der Waals forces and salt ions on the growth of water films on ice and the detachment of CO<sub>2</sub> bubbles. *EPL (Europhysics Letters)*, 113(4):43002, 2016.
- [32] M. Boström, O. I. Malyi, P. Thiyam, K. Berland, I. Brevik, C. Persson, and D. F. Parsons. The influence of Lifshitz forces and gas on premelting of ice within porous materials. *EPL (Europhysics Letters)*, 115(1):13001, 2016.
- [33] M. Elbaum and M. Schick. On the failure of water to freeze from its surface. *J. Phys. I France*, 1(12):1665–1668, 1991.
- [34] Mathias Boström, Oleksandr I. Malyi, Prachi Parashar, K. V. Shajesh, Priyadarshini Thiyam, Kimball A. Milton, Clas Persson, Drew F. Parsons, and Iver Brevik. Lifshitz interaction can promote ice growth at water-silica interfaces. *Phys. Rev. B*, 95:155422, Apr 2017.
- [35] D. E. Aspnes. Local field effects and effective medium theory: A microscopic perspective. *American Journal of Physics*, 50(8):704–709, 1982.
- [36] O. Bonnefoy, F. Gruy, and J.-M. Herri. A priori calculation of the refractive index of some simple gas hydrates of structures I and II. *Materials Chemistry and Physics*, 89(2):336 – 344, 2005.
- [37] O. Bonnefoy, F. Gruy, and J.-M. Herri. Van der Waals interactions in systems involving gas hydrates. *Fluid Phase Equilibria*, 231(2):176 – 187, 2005.
- [38] D. R. Lide, editor. *CRC Handbook of Chemistry and Physics (86th ed.)*. CRC Press, Boca Raton (FL), 2005.
- [39] M Ferdows and M Ota. Density of CO<sub>2</sub> Hydrate by Monte Carlo Simulation. *Proceedings of the Institution of Mechanical Engineers, Part C: Journal of Mechanical Engineering Science*, 220(5):691–696, 2006.
- [40] Y. Makogon. Natural gas hydrates – A promising source of energy. *Journal of Natural Gas Science and Engineering*, 2:49–59, 03 2010.
- [41] Drew Parsons and Barry W. Ninham. Importance of Accurate Dynamic Polarizabilities for the Ionic Dispersion Interactions of Alkali Halides. *Langmuir*, 26(3):1816–1823, 2010.
- [42] Johannes Fiedler, Priyadarshini Thiyam, Anurag Kurumbail, Friedrich A. Burger, Michael Walter, Clas Persson, Iver Brevik, Drew F. Parsons, Mathias Boström, and Stefan Y. Buhmann. Effective Polarizability Models. *The Journal of Physical Chemistry A*, 121(51):9742–9751, 2017. PMID: 29185741.
- [43] Claudia Hampel, Kirk A. Peterson, and Hans-Joachim Werner. A comparison of the efficiency and accuracy of the quadratic configuration interaction (QCISD), coupled cluster (CCSD), and Brueckner coupled cluster (BCCD) methods. *Chem. Phys. Lett.*, 190(1-2):1–12, 1992.
- [44] David E. Woon and Jr. Thom H. Dunning. Gaussian basis sets for use in correlated molecular calculations. III. The atoms aluminum through argon. *J. Chem. Phys.*, 98(2):1358–1371, 1993.
- [45] P. Thiyam, J. Fiedler, S. Y. Buhmann, C. Persson, I. Brevik, M. Boström, and D. F. Parsons. Ice Particles Sink below the Water Surface Due to a Balance of Salt, van der Waals, and Buoyancy Forces. *The Journal of Physical Chemistry C*, 122(27):15311–15317, 2018.
- [46] P. J. van Zwol, G. Palasantzas, and J. Th. M. De Hosson. Influence of dielectric properties on van der Waals/Casimir forces in solid-liquid systems. *Phys. Rev. B*, 79:195428, May 2009.
- [47] Nobuo Maeda. Is the Surface of Gas Hydrates Dry? *Energies*, 8(6):5361–5369, 2015.
- [48] Sebastian Hölz, Andrei Swidinsky, Malte Sommer, Marion Jegen, and Jörg Bialas. The use of rotational invariants for the interpretation of marine csem data with a case study from the north alex mud volcano, west Nile delta. *Geophysical Journal International*, 201(1):224–245, 2015.
- [49] A. P. Khain, N. BenMoshe, and A. Pokrovsky. Factors determining the impact of aerosols on surface precipitation from clouds: An attempt at classification. *Journal of the Atmospheric Sciences*, 65(6):1721–1748, 2008.